Journal of Molecular Spectroscopy 348 (2018) 57–63

Contents lists available at ScienceDirect

Journal of Molecular Spectroscopy

journal homepage: www.elsevier.com/locate/jms

Line-by-line spectroscopic parameters of HFC-32 ro-vibrational transitions within the atmospheric window around 8.2 μm

Nicola Tasinato [a,*], Giorgia Ceselin [a], Andrea Pietropolli Charmet [b], Paolo Stoppa [b], Santi Giorgianni [b]

[a] Scuola Normale Superiore, Piazza dei Cavalieri 7, I-56126 Pisa, Italy
[b] Dipartimento di Scienze Molecolari e Nanosistemi, Università Ca' Foscari Venezia, Via Torino 155, I-30172 Mestre (Venezia), Italy

ARTICLE INFO

Article history:
Received 15 August 2017
In revised form 7 December 2017
Accepted 23 December 2017
Available online 26 December 2017

Keywords:
Difluoromethane
Broadening coefficients
Spectroscopic line parameters
N_2–, O_2–, air-broadening
Greenhouse gases
Collisional cross sections

ABSTRACT

Difluoromethane (CH_2F_2,HFC-32) presents strong ro-vibrational bands within the 8–12 μm atmospheric window and hence it represents a greenhouse gas able of contributing to global warming. Numerous spectroscopic studies have been devoted to this molecule, however, much information on line-by-line parameters, like line intensities and broadening parameters, is still lacking. In this work, line-by-line spectroscopic parameters are retrieved for several CH_2F_2 ro-vibrational transitions belonging to the ν_7 band located around 8.5 μm. Self-broadening as well N_2– and O_2– broadening experiments are carried out at room temperature by using a tunable diode laser (TDL) spectrometer. The line shape analysis of CH_2F_2 self-broadened spectra leads to the determination of resonant frequencies, integrated absorption coefficients and self-broadening parameters, while CH_2F_2–N_2 and CH_2F_2–O_2 broadening coefficients are obtained from foreign-broadening measurements. In addition, the broadening parameters of CH_2F_2 in air are derived from the N_2– and O_2– broadening coefficients. The results of the present work provide fundamental information to measure the concentration profiles of this molecule in the atmosphere through remote sensing spectroscopic techniques.

1. Introduction

Since their introduction chlorofluorocarbons (CFCs) have been employed as propellants, refrigerants, blowing agents and fire extinguisher thanks to their favorable chemical and thermal properties. Nevertheless, CFCs contribute to the destruction of the stratospheric ozone layer and hence, with only a few exceptions, they have been phased out by the Montreal protocol. Among the replacement compounds, hydrofluorocarbons (HFCs) have been considered because of the absence of Cl atoms and the usually lower atmospheric lifetimes than CFCs. However, HFCs contribute to global climate changes since they behave as greenhouse gases. In fact, the C–F group strongly absorbs the infrared radiation within the 8–12 μm atmospheric window, thus altering the Earth's radiative budget. Therefore, the spectroscopic properties of HFCs are the subject of intensive research efforts, aimed at assessing their potential environmental impacts and at providing the required information for their atmospheric detection and modeling (e.g. see Refs. [1–3] and references therein).

For remote sensing spectroscopic applications, the work of laboratory spectroscopy is to provide accurate values of line-by-line spectroscopic parameters (i.e. transition frequencies, line intensities, pressure broadening and shifting coefficients and eventually, their temperature dependence) and absorption cross sections [4–6], the latter being particularly suitable for species presenting highly congested spectra. Furthermore, pressure broadening and shifting coefficients are strictly related to the intermolecular collisions and the potential driving them and hence their knowledge can provide important information about the chemical-physics of non-reactive scattering events and decay processes in the gas phase (see [7–14] and references therein). Clearly, for atmospheric purposes, the main collisional partners are N_2 and O_2. The line-by-line spectroscopic parameters and the absorption cross sections data of the species of interest are collected into a number of databases that are continuously updated in terms of spectral coverage, accuracy, chemical species and so on.

Among atmospheric trace gas pollutants, difluoromethane (CH_2F_2, HFC-32) is included in the HITRAN database [15], which lists cross-section data. This compound is employed in refrigerant mixtures together with CF_3CH_3, CF_3CH_2F, and CF_3CHF_2. Its atmospheric concentration has been determined to be around 3 ppt in 2005 [16], with a growing trend with respect to previous years. Because its environmental relevance, CH_2F_2 has been the subject of notable interest from the spectroscopic community (for an overview see [17–19] and references therein). Recently, the CH_2F_2

* Corresponding author.
E-mail address: nicola.tasinato@sns.it (N. Tasinato).

https://doi.org/10.1016/j.jms.2017.12.010
0022-2852/

adsorption over the TiO_2 surface has been studied by coupling diffuse reflectance infrared spectroscopy to periodic calculations rooted into density functional theory, being adsorption the first step involved in gas-phase heterogeneous catalysis aimed at removing atmospheric pollutants [20].

Focusing on absorption cross sections, Smith et al. determined the CH_2F_2 integrated absorbance cross sections over the 600–1900 cm^{-1} spectral range at different temperatures between 203 and 297 K [21], while few years later Beukes and Nicolaisen measured the intensity of the ν_4 fundamental band at six temperatures within the 212.5–297.0 K interval [22]. Meanwhile, integrated absorption cross sections were obtained with the aim of deriving the radiative forcing and global warming potential [23], and later on, they were re-investigated in the spectral region between 400 and 1600 cm^{-1} at 295 K by considering the effect of air broadening on the retrieved values [24]; more recently, the determination of integrated absorption cross sections was extended over the entire medium infrared region, up to 5000 cm^{-1} [17].

On the other hand, up to now only one study has dealt with the determination of pressure broadening coefficients of self-, N_2– and O_2-broadened CH_2F_2 [25]. The foreign broadening coefficients of the CH_2F_2 collisionally perturbed by different damping gases have been employed to derive the dissociation energy of the $(CH_2F_2)_2$ dimer and the experimental results have been benchmarked against predictions from different quantum mechanical methods [26,27].

Since line-by-line spectroscopic parameters assume particular relevance to acquire basic information for the atmospheric modeling of this compound and for remote sensing applications, this work aims at retrieving new data about self-, N_2–, and O_2– broadening coefficients of CH_2F_2 and integrated absorption coefficients. The focus is on lines from the ν_7 band, which, despite being weaker and less suited for satellite remote sensing than those from the ν_9 band, could offer useful information for atmospheric applications.

2. Experimental details

High-resolution IR spectra of CH_2F_2 perturbed by either itself or by N_2 and O_2 collisional partners were recorded by using a tunable diode laser (TDL) spectrometer [28] employing two different commercial lead salt lasers emitting within the atmospheric region and centered at 8.3 and 8.1 μm, respectively. All the measurements were carried out at room temperature (295 ± 1 K) with the spectrometer operating in a three beam configuration [29]: the first beam passed through the 68.2 (±0.2) cm absorption cell containing the CH_2F_2 sample; the other two beams were respectively sent to a Germanium etalon and a second cell filled with SO_2, both employed for calibration purposes. The three beams were collected by three different HgCdTe detectors, cryogenically cooled at liquid nitrogen temperature, and up to 1024 independent scans were averaged and digitized by a four-channel digital oscilloscope, resulting in spectra with a signal-to-noise ratio better than 1000. The acquired spectral micro-windows, about 0.3–0.5 cm^{-1} wide, were wavenumber calibrated by using the frequency of suitable SO_2 lines from high-resolution FTIR spectra [29], resulting in a calibration accuracy of ca. 4×10^{-4} cm^{-1} for unblended spectral lines. The transmittance spectra were obtained from the incident and transmitted radiation intensities according to the Beer-Lambert's law, with the incident intensity retrieved by fitting no absorption regions (i.e. the baseline) to a polynomial function.

For the self-broadening measurements, the sample pressure was varied in the range between 25 and 500 Pa, and each spectral micro-window was recorded up to 10 different pressures. For the foreign broadening measurements, spectra were recorded by using a fixed amount of CH_2F_2, around 100 Pa, depending on the intensities of the spectral lines, and increasing the total pressure up to 40 hPa. Pressure measurements were performed by means of the Alcatel ARD 1003 and 1002 capacitance vacuum gauges with a full scale range of 10 hPa and 100 hPa, respectively, each with quoted manufacturer's full scale accuracy of 0.15% and the pressure was found stable during the spectra recording well within 0.02 hPa and 0.2 hPa for self- and foreign-broadening experiments, respectively. Furthermore, following a well consolidated procedure [25,28,29], after checking single mode emission from the laser, the measurements were performed by removing the monochromator to avoid instrumental distortions. A complete equilibration inside the cell was achieved by adopting a 15 min delay between the filling and the recording of the corresponding spectrum. Gas handling operations were performed by using a stainless steel vacuum line and before each measurement, the cell was evacuated to about 10^{-4} Pa by means of a diffusion pump backed by a double stage rotary pump. The CH_2F_2 sample was purchased by Aldrich with a stated purity of 99.7%, and it was used without any further purification. To retrieve line-by-line spectroscopic parameters, the recorded absorption features were fitted by using the VLSF program operating in the multiline mode [30]. Assignment of the spectral lines was performed on the basis of Ref. [19].

3. Results and discussion

The CH_2F_2 molecule belongs to the C_{2v} symmetry point group and it is a near prolate asymmetric rotor as confirmed by the Ray's asymmetry parameter $\kappa = -0.93$. It possesses nine normal modes of vibration which can be classified as belonging to A_1 (ν_1–ν_4), A_2 (ν_5), B_1(ν_6, ν_7) or B_2 (ν_8, ν_9) symmetry species. The IR spectrum in the 1000–1300 cm^{-1} atmospheric spectral region is characterized by the absorptions of the ν_3, ν_5, ν_7 and ν_9 fundamental vibrations, which correspond to the CF_2 symmetric stretching, CH_2 twisting, CH_2 rocking and CF_2 asymmetric stretching vibrations, respectively. The corresponding excited vibrational levels form, together with the $\nu_4 = 2$ level, a resonant pentad interacting through Coriolis and anharmonic resonances [19]. Because of these interactions the ν_5 vibration, which is expected to be inactive in the IR, gives rise to a weak band centered at 1255.85851 cm^{-1}. Among the remaining fundamental bands within the atmospheric window, ν_9 produces the most intense absorption of the whole CH_2F_2 IR spectrum centered at 1090.126362 cm^{-1}. It is overlapped with the ν_3 band at 1111.516271 cm^{-1}, whose R branch is, in turn severely blended with the absorption of the ν_7 fundamental resonating at 1178.641412 cm^{-1}. These bands are expected to produce transitions in the P, Q and R branches classifiable as even ($K''_a + K''_c = J''$) and odd ($K''_a + K''_c = J'' + 1$) sub-bands.

The spectral range covered by the TDL spectrometer matches the ro-vibrational lines stemming from the ν_7 normal mode and, of these 5, 20 and 35 belong to the P, Q and R branch, respectively. Because the lasers employed for the measurements present a Lorentzian instrumental line shape function, the spectral lines have been fitted to the Voigt profile. During the fits, the Gaussian half widths have been fixed to the molecular contribution $\gamma_D^{CH_2F_2}$ given by

$$\gamma_D^{CH_2F_2} = \frac{\nu_{if}}{c}\left(\frac{2k_B N_a T \ln 2}{m}\right)^{1/2} \quad (1)$$

where ν_{if} is the frequency of the $f \leftarrow i$ ro-vibrational transition, c represents the speed of light, k_B is the Boltzman's constant, N_a is the Avogadro's constant, T is the absolute temperature and m is the mass of the radiating species. An example of the fits performed during self-broadening measurements is given in Fig. 1, showing the spectral region between 1221.30 and 1221.67 cm^{-1}, while Fig. 2 presents the CH_2F_2 spectrum perturbed by similar amounts

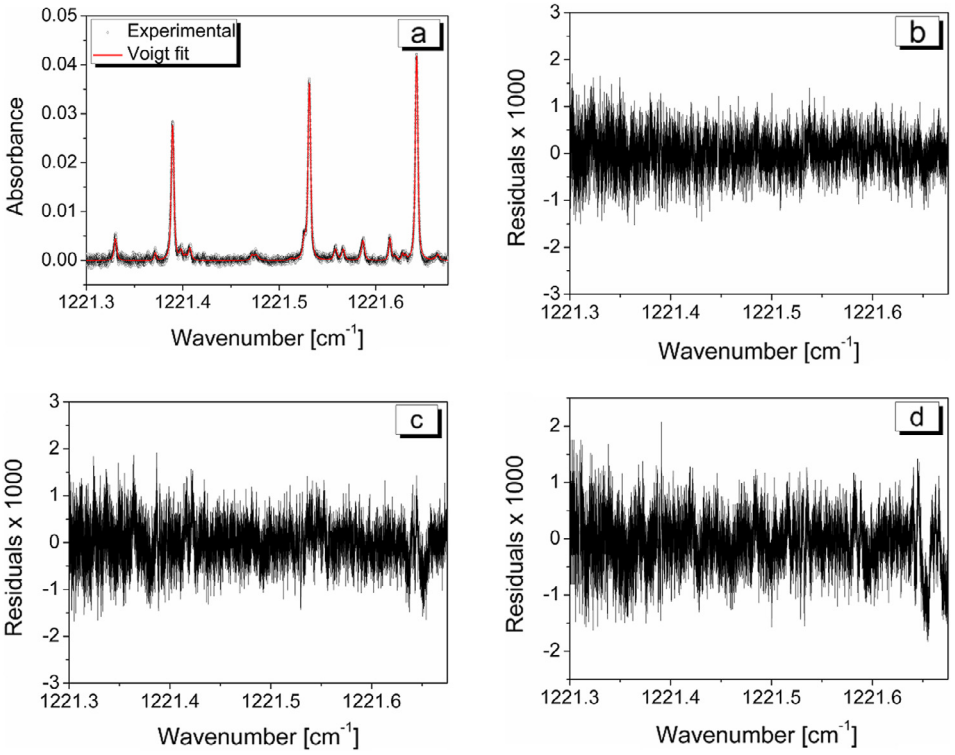

Fig. 1. (a) High resolution spectrum of self-broadened CH_2F_2 between 1221.30 and 1221.67 cm^{-1} (CH_2F_2 pressure = 123.0 Pa; optical path = 68.2 cm; T = 295 K) showing the synthetic trace obtained by employing the Voigt profile. (b) Residuals for CH_2F_2 pressure = 46.1 Pa. (c) Residuals for CH_2F_2 pressure = 123.0 Pa. (d) Residuals for CH_2F_2 pressure = 401.1 Pa.

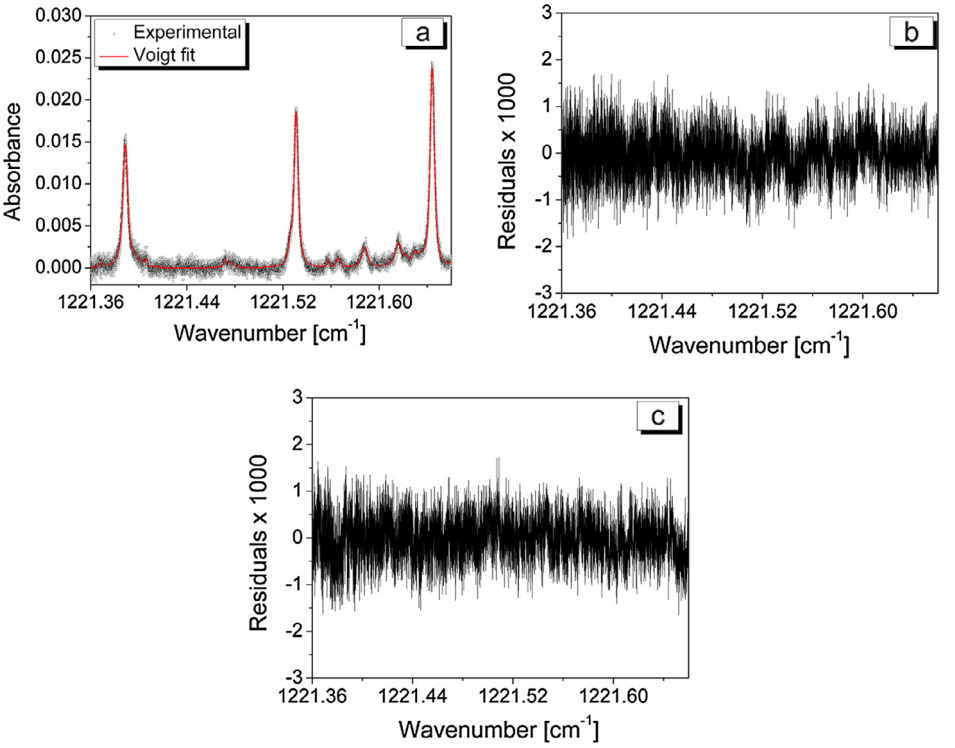

Fig. 2. High-resolution IR spectrum of CH_2F_2 between 1221.36 and 1221.66 cm^{-1} perturbed by similar amounts of O_2 and N_2 damping gases. Experimental spectrum and synthetic trace obtained using the Voigt profile (CH_2F_2 partial pressure = 99.4 Pa; N_2 partial pressure = 941 Pa; optical path = 68.2 cm; T = 295 K). (b) Residuals of the fit for N_2 partial pressure = 941 Pa. (c) Residuals of the fit for O_2 partial pressure = 881 Pa.

of O_2 and N_2 damping gases, about 900 Pa, in the 1221.36 and 1221.66 cm^{-1} range. These figures illustrate two important aspects concerning the line shape analysis performed on the high resolution spectra of CH_2F_2. The first one is the presence of many weak features that make the spectrum very crowded, with a density of about 45 lines/cm^{-1}. In fact, some of the weaker absorptions are due to the hot bands originating from the $\nu_4 = 1$ state that at room temperature has a population of ca. 13% with respect to the ground state. The second aspect is that the Voigt profile model well reproduces both the self-broadened and the foreign broadened spectra within the experimental conditions, as expected on the basis of previous investigations. Under this point of view, it should be noted that the experimental conditions adopted coupled to the high density of lines make the use of refined line shape models, accounting for narrowing effects, to give no improvements on the retrieved parameters, also in view of their computational cost, an aspect already pointed out in previous investigations [31–33]. During the fits of the recorded spectra, resonant frequencies (ν_0), Lorentzian (i.e. collisional) half width (Γ_L) and line intensities (S) have been refined. Self-broadening experiments have led to the determination of self-broadening coefficients (γ^0_{self}) and integrated absorption coefficients (S^0) by a weighted linear fit (according to the reciprocal of the squared errors derived from the line shape analysis) of the collisional half widths and line intensities against the pressure of $P_{CH_2F_2}$, respectively:

$$\Gamma_L = \Gamma_0 + \gamma^0_{self} \times P_{CH_2F_2} \quad (2)$$

$$S = S^0 \times P_{CH_2F_2} \quad (3)$$

where Γ_0 takes into account the broadening due to the Lorentzian instrumental line shape function. Examples concerning the pressure dependence of the collisional half width and the line intensity of the $20_{11,9} \leftarrow 19_{10,9}$ ro-vibrational transition centered at 1221.6437 cm^{-1}, and the corresponding linear fits, are given in Fig. 3a and b, respectively.

Foreign broadening experiments have led to the determination of CH_2F_2–N_2 ($\gamma^0_{N_2}$) and CH_2F_2–O_2 ($\gamma^0_{O_2}$) broadening coefficients, which have been obtained by a weighted linear fit as in Eq. (2), with the only difference that, in this case, Γ_0 accounts for both the instrumental broadening and the self-broadening contributions. The linear fits carried out for retrieving the foreign broadening parameters of the $20_{11,9} \leftarrow 19_{10,9}$ transition of the ν_7 band are reproduced in Fig. 4.

The line-by-line parameters obtained for the ν_7 band transitions of CH_2F_2 analyzed in the present work are collected in Table 1, where the CH_2F_2–air broadening coefficients are also reported.

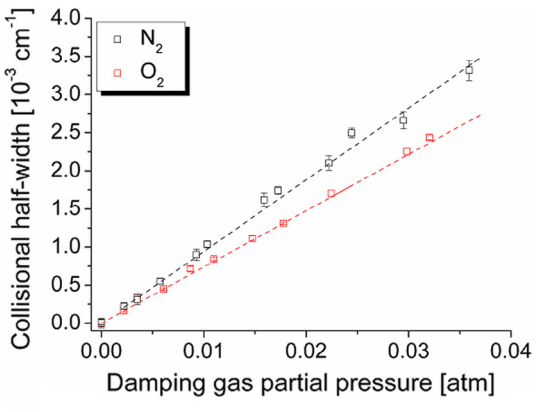

Fig. 4. Linear fits for retrieving N_2– and O_2-broadening coefficients for the $20_{11,9} \leftarrow 19_{10,9}$ ro-vibrational transition of the ν_7 band (squares: experimental half widths; dotted straight lines: linear fit of Lorentzian half widths against the damping gas partial pressure). The contribution due to self- and instrumental broadening has been subtracted.

These have been obtained from the measured N_2– and O_2– broadening coefficients according to the usual equation

$$\gamma^0_{air} = 0.79\gamma^0_{N_2} + 0.21\gamma^0_{O_2}. \quad (4)$$

From Table 1 it can be noted that CH_2F_2 self-broadening coefficients range from 0.30 cm^{-1} atm^{-1} to 0.66 $cm^{-1}atm^{-1}$ and take an average value of 0.51 ± 0.09 $cm^{-1}atm^{-1}$, thus confirming our previous findings based on a smaller subset of data [25]. In passing, it should be noted that, as in the case of other asymmetric top molecules [10,34], collisional coupling may affect the measured line shapes, particularly when even and odd doublets are degenerate, thus reducing the broadening of the spectral lines and hence leading to smaller broadening coefficients. This phenomenon arises because the unresolved K doublets are composed by two lines, namely $J'_{K'_aK'_c} \leftarrow J''_{K''_aK''_c}$ and $J'_{K'_aK'_c+1} \leftarrow J''_{K''_aK''_c+1}$, which are separated by a frequency smaller than the collisional line width. When this condition is met, collisions may cause coupling between pairs of optical transitions, and population is exchanged between their initial and final states. Concerning N_2– and O_2– broadening coefficients, they vary from 0.061 cm^{-1} atm^{-1} to 0.127 cm^{-1} atm^{-1} and from 0.045 cm^{-1} atm^{-1} to 0.085 cm^{-1} atm^{-1}, respectively.

For twenty-six transitions, it is possible to compare the present results with those determined in a previous work [25]. Concerning transition frequencies, we note an overall good agreement between the two sets of data, with deviations lower or comparable

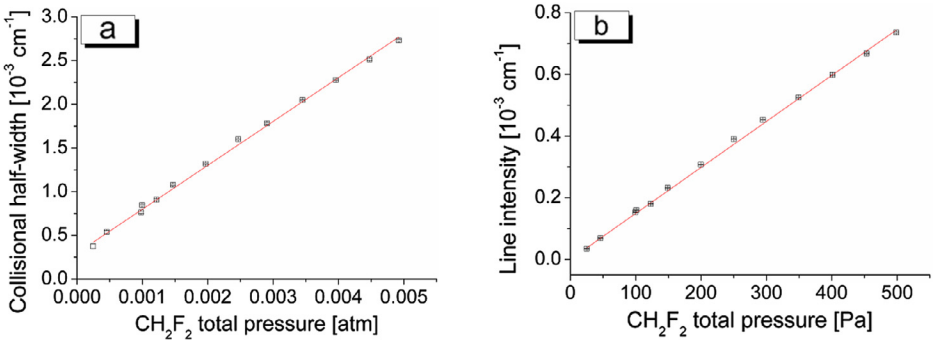

Fig. 3. (a) Self-broadening of the $20_{11,9} \leftarrow 19_{10,9}$ ro-vibrational transition belonging to the ν_7 band of CH_2F_2, centered at 1221.6437 cm^{-1} (squares: experimental half widths; straight line: linear fit of Lorentzian half widths against the CH_2F_2 total pressure). Error bars are shown and are three times the uncertainties retrieved from line profile analysis. (b) Linear fit leading to the integrated absorption coefficient of the $20_{11,9} \leftarrow 19_{10,9}$ ro-vibrational transition of CH_2F_2 (squares: experimental line intensities; straight line: linear fit of line intensities against the CH_2F_2 total pressure). Error bars are shown and are three times the uncertainties retrieved from line profile analysis.

Table 1
Assignment, transition frequency, integrated absorption coefficient, self-, nitrogen-, oxygen- and air-broadening coefficients for CH_2F_2 transitions belonging to the ν_7 band.[a]

J'	K'_a	K'_c	J''	K''_a	K''_c	ν_0 [cm^{-1}]	S^0 [10^{-22} cm molecule^{-1}]	γ_{self} [cm^{-1} atm^{-1}]	γ_{N_2} [cm^{-1} atm^{-1}]	γ_{O_2} [cm^{-1} atm^{-1}]	γ_{air} [cm^{-1} atm^{-1}]
18	2	17	17	1	17	$1197.36528_0(6_0)$	$1.7_2(1_2)$	$0.490_7(6_3)$	$0.070_1(4_1)$	$0.053_5(2_3)$	$0.066_6(3_7)$
39	8	31	39	7	33	$1197.41165_3(4_9)$	$0.86_0(7_2)$	$0.389_7(8_6)$	$0.073_2(4_6)$	$0.045_0(3_3)$	$0.067_3(4_3)$
23	4	20	23	1	22	$1197.4496_9(2_8)$	$0.343_6(7_2)$	$0.30_2(2_6)$	/	/	/
38	8	31	38	7	31	$1197.47817_1(7_9)$	$0.85_8(6_1)$	$0.51_8(2_2)$	$0.109_5(2_6)$	$0.064_2(2_4)$	$0.100_0(2_6)$
10	5	5	9	4	5	$1197.52355_0(9_2)$[b]	$5.4_6(4_4)$	$0.571_1(6_1)$	$0.089_8(8_1)$	$0.069_7(6_0)$	$0.0856(7_7)$
38	8	30	38	7	32	$1197.53165_3(5_5)$	$0.52_7(6_4)$	$0.56_4(3_3)$	$0.073_0(5_3)$	$0.064_0(4_3)$	$0.071_1(5_1)$
20	12	8	21	11	10	$1197.58201_0(5_7)$[b]	$0.56_4(5_3)$	$0.43_2(1_7)$	/	/	/
10	3	7	9	0	9	$1197.59039_0(9_9)$	$0.12_7(5_1)$	$0.45_4(1_4)$	/	/	/
19	1	18	18	0	18	$1197.6021_1(1_3)$	$1.9_3(2_0)$	$0.530_5(7_4)$	$0.112_2(5_1)$	$0.0760_8(8_0)$	$0.104_6(4_2)$
37	8	30	37	7	30	$1197.6133_4(1_7)$	$0.42_7(8_7)$	$0.39_9(2_9)$	$0.071_0(6_6)$	$0.068_0(5_4)$	$0.062_4(6_4)$
15	4	11	14	3	11	$1197.6409_6(1_2)$	$4.0_3(2_7)$	$0.577_6(5_6)$	$0.108_2(2_2)$	$0.0779_8(5_5)$	$0.101_9(1_8)$
37	8	29	37	7	31	$1197.6515_1(1_8)$	$0.79_7(3_8)$	$0.44_8(2_5)$	$0.077_3(7_1)$	$0.071_3(6_1)$	$0.076_0(6_9)$
43	4	39	42	5	37	$1197.6940_8(3_2)$	$0.151_2(5_2)$	$0.42_9(6_0)$	/	/	/
36	8	29	36	7	29	$1197.74212(1_2)$	$0.72_6(5_6)$	$0.457_2(9_8)$	$0.081_8(4_4)$	$0.069_9(5_9)$	$0.079_3(4_7)$
21	3	18	20	2	18	$1197.76033_0(7_6)$	$4.8_2(2_8)$	$0.533_3(5_4)$	$0.106_8(5_6)$	$0.081_5(1_0)$	$0.101_5(4_6)$
36	8	28	36	7	30	$1197.7685_1(1_3)$	$0.44_4(5_9)$	$0.41_5(5_9)$	$0.091_5(8_0)$	$0.0590_0(6_0)$	$0.084_7(6_4)$
24	4	21	24	1	23	$1197.7997_6(2_9)$	$0.221_2(4_0)$	$0.41_5(2_8)$	/	/	/
24	13	11	25	12	13	$1197.82663_5(7_1)$[b]	$0.26_3(2_6)$	$0.64_5(4_2)$	/	/	/
15	4	12	14	3	12	$1197.8357_7(1_2)$	$2.5_1(1_2)$	$0.575_5(9_3)$	$0.104_5(6_1)$	$0.072_0(1_6)$	$0.097_7(5_1)$
6	6	0	5	5	0	$1197.86850_3(9_0)$[b,c]	$7.3_0(1_2)$	$0.609_1(4_7)$	$0.098_2(2_4)$	$0.078_4(2_4)$	$0.094_1(2_4)$
35	8	27	35	7	29	$1197.8826_9(1_4)$[d]	$4.3_6(4_2)$	$0.51_1(1_6)$	$0.111_5(1_4)$	$0.061_3(1_7)$	$0.101_0(1_5)$
18	3	16	17	2	16	$1197.88274_7(3_8)$[e]	$4.3_5(3_4)$	$0.50_9(1_2)$	$0.095_3(8_1)$	$0.073_8(1_1)$	$0.090_8(6_6)$
21	2	19	21	1	19	$1197.98169_9(7_2)$[f]	$4.9_9(3_1)$	$0.556_7(5_2)$	$0.104_3(7_0)$	$0.0760_3(3_7)$	$0.971_6(6_3)$
34	8	26	34	7	28	$1197.99397_0(6_1)$	$0.59_9(4_4)$	$0.40_6(1_9)$	$0.087_1(3_9)$	$0.074_0(1_1)$	$0.084_4(3_3)$
15	11	4	16	10	6	$1198.07018_0(7_3)$[b]	$0.20_2(2_0)$	$0.41_3(2_7)$	/	/	/
33	8	26	33	7	26	$1198.09423_3(1_5)$	$0.51_9(4_6)$	$0.49_4(1_5)$	$0.087_2(2_9)$	$0.070_1(4_6)$	$0.083_6(3_3)$
33	8	25	33	7	27	$1198.1022_8(1_1)$	$1.27_0(5_9)$	$0.545_1(7_4)$	$0.090_2\ (3_7)$	$0.072_2(1_2)$	$0.086_4(3_2)$
11	5	6	10	4	6	$1198.15214_0(7_0)$[b]	$7.0_7(2_2)$	$0.570_7(6_4)$	$0.115_9(5_3)$	$0.0789_1(9_2)$	$0.108_1(4_4)$
16	4	12	15	3	12	$1198.19049_7(1_5)$	$2.9_0(1_2)$	$0.56_7(1_6)$	$0.127_0(2_1)$	$0.085_0(1_0)$	$0.118_2(1_9)$
32	8	25	32	7	25	$1198.20224_7(8_1)$	$1.7_7(2_3)$	$0.557_6(6_2)$	$0.097_2(9_0)$	$0.0804_6(8_5)$	$0.936_8(7_3)$
32	8	24	32	7	26	$1198.20769_0(2_7)$	$0.90_3(6_9)$	$0.66_1(3_1)$	$0.102_6(9_7)$	$0.079_2(2_2)$	$0.097_7(8_1)$
11	9	2	11	8	4	$1202.6970_6(1_1)$[b]	$1.7_4(2_4)$	$0.49_7(3_1)$	$0.083_9(1_4)$	$0.074_7(4_1)$	$0.082_0(2_0)$
9	7	2	8	6	2	$1202.72343_9(7_4)$[b]	$6.8_4(4_4)$	$0.554_9(9_9)$	$0.098_5(3_9)$	$0.072_6(2_3)$	$0.093_1(3_6)$
10	9	1	10	8	3	$1202.73245_9(6_7)$[b]	$1.6_3(1_6)$	$0.60_0(4_9)$	$0.100_3(5_3)$	$0.077_1(5_4)$	$0.095_4(5_3)$
27	3	24	26	2	24	$1202.74265_6(1_8)$	$2.71_8(7_9)$	$0.60_1(1_4)$	$0.098_2(5_0)$	$0.072_6(4_2)$	$0.092_8(4_9)$
14	6	8	13	5	8	$1202.91639_9(3_6)$[b]	$6.2_8(4_4)$	$0.595_8(9_3)$	$0.102_2(6_7)$	$0.074_3(2_6)$	$0.096_3(5_8)$
24	1	23	23	0	23	$1202.9308_1(1_1)$	$0.59_4(1_3)$	$0.46_0(3_1)$	/	/	/
26	4	22	25	3	22	$1202.95887_2(4_3)$	$1.80_8(8_8)$	$0.46_9(1_4)$	$0.070_9(5_3)$	$0.053_6(3_9)$	$0.067_3(5_0)$
24	3	22	23	2	22	$1202.98587_0(7_8)$	$1.8_6(1_5)$	$0.50_7(1_2)$	$0.076_6(6_9)$	$0.060_7(2_6)$	$0.073_2(6_0)$
19	5	14	18	4	14	$1202.99997_0(3_8)$	$3.36_0(7_5)$	$0.551_7(6_6)$	$0.081_5(2_6)$	$0.069_7(2_1)$	$0.079_0(2_5)$
19	5	15	18	4	15	$1203.06831_5(7_6)$	$2.12_2(9_1)$	$0.50_3(1_7)$	$0.079_9(4_2)$	$0.070_6(1_6)$	$0.077_9(3_7)$
23	4	20	22	3	20	$1203.16559_9(3_5)$	$3.14_4(3_7)$	$0.54_3(1_1)$	$0.089_1(1_0)$	$0.071_8(1_8)$	$0.085_5(1_2)$
25	15	10	26	14	12	$1203.23767_9(9_0)$[b]	$0.31_2(3_9)$	$0.58_4(1_8)$	$0.108_8(8_2)$	$0.062_0(4_3)$	$0.099_0(7_4)$
44	10	35	44	9	35	$1203.2538_3(2_7)$[b]	$0.251_0(5_6)$	$0.33_2(1_4)$	/	/	/
29	16	13	30	15	15	$1203.3021_1(4_5)$[b]	$0.249_3(8_2)$	$0.37_3(2_5)$	/	/	/
10	7	3	9	6	3	$1203.3554_5(1_1)$[b]	$7.11_6(6_9)$	$0.571_8(8_1)$	$0.100_5(1_8)$	$0.0733_8(8_2)$	$0.094_8(1_6)$
35	4	32	34	3	32	$1212.9828_1(1_3)$	$0.43_1(4_7)$	$0.59_2(2_2)$	$0.092_9(6_3)$	$0.072_8(3_9)$	$0.088_7(5_8)$
31	6	26	30	5	26	$1212.98804_1(5_2)$	$0.756_4(5_7)$	$0.35_3(3_0)$	/	/	/
26	7	19	25	6	19	$1213.04784_1(1_9)$[b]	$0.97_0(5_8)$	$0.57_4(2_0)$	$0.068_3(6_4)$	$0.0508_1(7_3)$	$0.064_6(5_2)$
11	10	1	10	9	1	$1213.05226_0(3_1)$[b]	$6.0_5(1_1)$	$0.510_4(8_5)$	$0.098_7(4_3)$	$0.0780_3(5_0)$	$0.094_3(3_5)$
16	9	7	15	8	7	$1213.08295_6(4_0)$[b]	$3.5_2(5_0)$	$0.53_4(1_1)$	$0.090_7(2_8)$	$0.077_2(2_7)$	$0.087_9(2_8)$
21	8	13	20	7	13	$1213.09044_3(5_0)$[b]	$4.24_0(8_5)$	$0.621_8(7_1)$	$0.103_4(2_6)$	$0.085_2(4_8)$	$0.099_6(3_0)$
32	6	26	31	5	26	$1213.09904_5(6_1)$	$0.43_5(6_1)$	$0.52_3(3_9)$	$0.092_2(4_7)$	$0.079_1(7_7)$	$0.089_4(5_4)$
16	15	2	16	14	2	$1221.3299_8(3_1)$[b]	$0.203_6(4_1)$	$0.32_0(2_2)$	/	/	/
30	9	21	29	8	21	$1221.3891_6(2_8)$[b]	$1.4_9(1_1)$	$0.619_7(7_6)$	$0.090_9(8_4)$	$0.072_3(4_2)$	$0.087_0(7_5)$
41	7	35	40	6	35	$1221.5257_0(2_5)$	$0.185_1(4_6)$	$0.38_5(3_5)$	/	/	/
25	10	15	24	9	15	$1221.53119_3(5_1)$[b,g]	$1.71_1(9_3)$	$0.559_3(7_5)$	$0.090_8(7_2)$	$0.073_8(2_1)$	$0.087_1(6_1)$
43	7	36	42	6	36	$1221.6149_5(4_8)$	$0.189_4(5_0)$	$0.43_5(3_0)$	/	/	/
20	11	9	19	10	9	$1221.6437_6(8_0)$[b]	$2.05_6(2_8)$	$0.502_5(6_8)$	$0.094_0(2_1)$	$0.073_4(1_2)$	$0.089_7(1_9)$
24	12	12	23	11	12	$1227.13560_1(2_2)$[b]	$1.00_0(3_8)$	$0.404_2(8_6)$	$0.090_3(5_5)$	$0.071_5(2_7)$	$0.086_3(4_9)$

[a] Figures in parentheses are statistical errors in the units of the last significant digits.
[b] Even and odd components of the transition.
[c] Overlapped with the $35_{8,28} \leftarrow 35_{7,28}$ transition.
[d] Overlapped with the $18_{3,16} \leftarrow 17_{2,16}$ transition.
[e] Overlapped with the $35_{8,27} \leftarrow 35_{7,29}$ transition.
[f] Overlapped with the $34_{8,27} \leftarrow 34_{7,27}$ transition.
[g] Overlapped with the $41_{7,35} \leftarrow 40_{6,35}$ transition.

to the accuracy of the calibration. Exceptions occur for eight transitions ($10_{5,5} \leftarrow 9_{4,5}$; $38_{8,30} \leftarrow 38_{7,32}$; $20_{12,8} \leftarrow 21_{11,10}$; $19_{1,8} \leftarrow 18_{0,8}$; $37_{8,30} \leftarrow 37_{7,30}$; $15_{4,11} \leftarrow 14_{3,11}$; $37_{8,29} \leftarrow 37_{7,31}$; $21_{3,18} \leftarrow 20_{2,18}$) for which the differences are larger than 1.5×10^{-3} cm^{-1}. This is likely due to the fact that these transitions are affected by the overlaps with neighboring lines. Furthermore, they usually lie at the beginning of the laser emission mode, and hence they are located in the region of lowest signal-to-noise ratio of the laser emission profile. In fact, they are also associated to some of the largest deviations, up to 27%, for line intensities. From a general point

of view, the agreement with previous measurements is good, around 10%, and it reflects the statistical errors affecting the intensities. In passing, it should be noted that in Ref. [25] there is a typo in the value reported for the $37_{8,30} \leftarrow 37_{7,30}$ transition intensity (0.253×10^{-22} cm molecule^{-1}), the correct one being $0.52_3(1_3) \times 10^{-22}$ cm molecule^{-1}. Concerning self-broadening coefficients, the agreement between the two datasets is good, on average within 6% and in general within 10%. The largest discrepancies of 21% and 25% are for the transitions $38_{8,30} \leftarrow 38_{7,32}$ and $36_{8,28} \leftarrow 36_{7,30}$, respectively. Yet, the values here determined provide a smoother variation of the self-broadening coefficients with the J'' quantum number within the $K_a'' = 7$ subbranch, and hence they are expected to be more reliable. The situation for N_2– and O_2–broadening coefficients is more involved and there is a larger number of data that presents deviations above 15%, particularly in the case of collisions between CH_2F_2 and O_2. This is not surprising considering that broadening parameters are strongly affected by the location of the baseline. In particular, it has been pointed out that an error in the base of 1% may cause an error of 12% in the retrieved Lorentzian line-width [35]. Due to the high density of transitions in the spectra analyzed and the line overlaps induced by the pressurization with the buffer gas, the location of the base line can be expected to be the main source of uncertainty in the retrieved foreign broadening coefficients, an aspect that is only partially accounted for in the errors reported in Table 1, which are of statistical nature. While the N_2– and O_2– broadening coefficients here determined appear consistent in view of the smoother variation with respect to the rotational quantum numbers, a conservative estimate of their uncertainty is 10–15%, which, taken into account the difficulty in the analysis caused by the spectral congestion, appears more than satisfactory.

From the collisional cross sections obtained experimentally, it has been possible to obtain some hints about the K_a dependence of R-branch transitions and the J dependence for Q-type transitions belonging to the $K_a'' = 7$ sub-branch. The observed trends are illustrated in Figs. 5 and 6, respectively. In the case of the self-broadening of R-branch transitions, Fig. 5 suggests an initial increase of the broadening efficiency with the K_a quantum number, up to $K_a'' \approx 5$, and then a decrease as K_a'' raises further. As expected, the K_a dependence of N_2– and O_2-broadening parameters is much weaker, and within the K_a-range here investigated, they keep an almost constant value around 0.094 ± 0.012 and 0.0718 ± 0.0095 cm^{-1} atm^{-1}, respectively. The J-dependence of self-broadening coefficients for Q-branch transitions belonging to the $K_a'' = 7$ sub-bands is more involved: from Fig. 6, it can be speculated that they have the tendency to decrease with increasing J'', at least within the range $32 \leq J'' \leq 39$. Concerning the CH_2F_2–N_2 and CH_2F_2–O_2 collisional cross sections, the dependence on J is very weak,

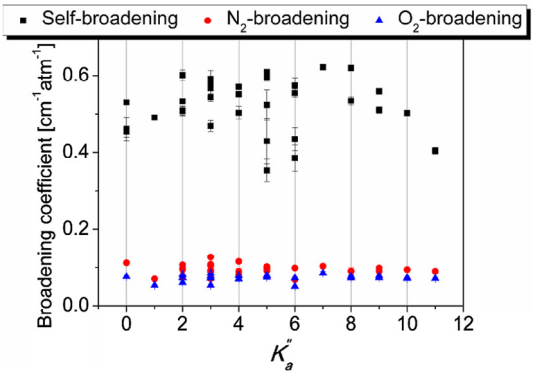

Fig. 5. Dependence of self-, N_2– and O_2– broadening coefficients on the K_a pseudo-quantum number for CH_2F_2 ro-vibrational transitions belonging to the R-branch of the ν_7 band.

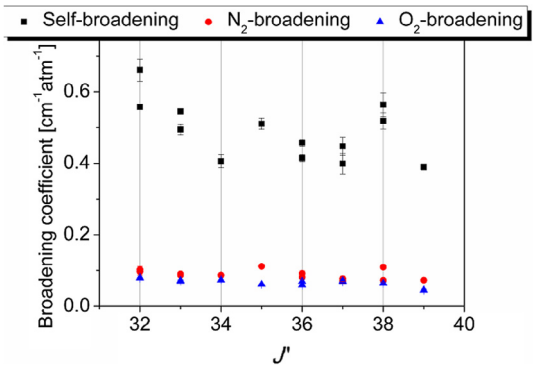

Fig. 6. Dependence of self-, N_2– and O_2– broadening coefficients on the J quantum number for CH_2F_2 Q-branch ro-vibrational transitions belonging to the $K_a'' = 7$ manifold of the ν_7 band.

although the efficiency of collisions in broadening the spectral lines seems to decrease as J'' increases. However, it should be pointed out that the trend suggested for this dependence has to be considered as indicative, since the J-range accessed by the present measurements is quite small, to allow definitive conclusion.

4. Conclusion

Spectroscopic parameters are crucial elements for remote sounding techniques and for understanding of the Earth's atmospheric properties, also in relation to global climate changes caused by anthropogenic activities. Under this point of view, HFCs represent trace gas pollutants that are able to alter the Earth's radiative balance thus contributing to global warming. In the present work, the line shape parameters of difluoromethane have been determined for several ro-vibrational transitions within the atmospheric window region around 8.2–8.3 μm. The measurements have been carried out exploiting tunable diode laser spectroscopy by perturbing CH_2F_2 by itself, as well as by the atmospherically relevant buffer gasses N_2 and O_2. The recorded transitions belong to the ν_7 band, which is one of the strongest bands of the CH_2F_2 IR spectrum, and the study has been complicated by the high-density of lines in the high resolution spectra of this molecule. In spite of this, the line profile analysis has led to the determination, for 60 lines, of resonant frequencies, integrated absorption coefficients (i.e. line intensities) and self-, N_2– and O_2-broadening coefficients. In addition, from the measured N_2– and O_2– broadening parameters, the broadening coefficients of CH_2F_2 in air have been derived. Finally, from the obtained collisional cross sections some indications about their quantum number dependence have been drawn.

As a concluding remark it is worth pointing out that, despite the complication arising from the spectral congestion, studies aiming at the determination of CH_2F_2 broadening parameters should be encouraged, because this molecule actually represents an important atmospheric trace gas pollutants. For this reason it has been widely investigated by the spectroscopic community, in both the IR and MW spectral regions, with the aim of understanding the rotational/vibrational energy level patterns and deriving set of spectroscopic parameters for simulating its spectra, while very little work has been devoted to broadening parameters, with the present contribution being an effort for bridging this gap.

Acknowledgments

The present work has been financially supported by MIUR (PRIN 2012 fund for project STAR: "Spectroscopic and Computational Techniques for Astrophysical and Atmospheric Research", prot.

no. 20129ZFHFE_003 and PRIN 2015 funds for project STARS in the CAOS: Simulation Tools for Astrochemical Reactivity and Spectroscopy in the Cyberinfrastructure for Astrochemical Organic Species, cod. 2015F59J3R), Università Ca' Foscari Venezia (ADiR funds), and Scuola Normale Superiore (funds for project COSMO: "Combined experimental and computational spectroscopic modeling for astrochemical applications"). GC thanks Scuola Normale Superiore for her research fellowship.

References

[1] D. McNaughton, E.G. Robertson, D. Thompson, T. Chimdi, M.K. Bane, D. Appadoo, J. Anal. Chem. 82 (2010) 7958–7964.
[2] N. Tasinato, P. Stoppa, A. Pietropolli Charmet, S. Giorgianni, A. Gambi, J. Quant. Spectrosc. Radiat. Transfer 113 (2012) 1240–1249.
[3] N. Tasinato, D. Moro, P. Stoppa, A. Pietropolli Charmet, P. Toninello, S. Giorgianni, Appl. Surf. Sci. 353 (2015) 986–994.
[4] J. Demaison, K. Sarka, E.A. Cohen, Spectroscopy from Space, Kluwer Academic Publisher, Dordrecht, 2001.
[5] G. Duxbury, Infrared Vibration-Rotation Spectroscopy, John Wiley & Sons, Chichester, 2000.
[6] G. Duxbury, N. Langford, K. Hay, N. Tasinato, J. Mod. Opt. 56 (2009) 2034–2048.
[7] J.M. Hartmann, C. Boulet, D.C. Robert, Collisional Effects on Molecular Spectra, Elsevier, New York, 2008.
[8] D. Robert, J.M. Thuet, J. Bonamy, S. Temkin, Phys. Rev. A 47 (1993) R771–R773.
[9] F. Rohart, H. Mäder, H.W. Nicolaisen, J. Chem. Phys. 101 (1994) 6475–6486.
[10] G. Cazzoli, L. Cludi, G. Cotti, C. Degli Esposti, G. Buffa, O. Tarrini, J. Chem. Phys. 102 (1995) 1149–1156.
[11] J.-M. Hartmann, J.P. Bouanich, K.W. Juks, G. Blanque, J. Walrand, D. Bermejo, J.-L. Domenech, N. Lacome, J. Chem. Phys. 110 (1999) 1959–1968.
[12] N. Tasinato, G. Duxbury, N. Langford, K.G. Hay, J. Chem. Phys. 132 (2010) 044316.
[13] N. Tasinato, K.G. Hay, N. Langford, G. Duxbury, D. Wilson, J. Chem. Phys. 132 (2010) 164301.
[14] G. Duxbury, N. Tasinato, K. Hay, D. Wilson, N. Langford, AIP Conf. Proc. 1290 (2010) 194–203.
[15] I.E. Gordon, L.S. Rothman, C. Hill, R.V. Kochanov, Y. Tan, P.F. Bernath, M. Birk, V. Boudon, A. Campargue, K.V. Chance, B.J. Drouin, J.-M. Flaud, R.R. Gamache, J.T. Hodges, D. Jacquemart, V.I. Perevalov, A. Perrin, K.P. Shine, M.-A.H. Smith, J. Tennyson, G.C. Toon, H. Tran, V.G. Tyuterev, A. Barbe, A.G. Császá, V.M. Devi, T. Furtenbacher, J.J. Harrison, J.-M. Hartmann, A. Jolly, T.J. Johnson, T. Karman, I. Kleiner, A.A. Kyuberis, J. Loos, O.M. Lyulin, S.T. Massie, S.N. Mikhailenko, N. Moazzen-Ahmadi, H.S.P. Müller, O.V. Naumenko, A.V. Nikitin, O.L. Polyansky, M. Rey, M. Rotger, S.W. Sharpe, K. Sung, E. Starikova, S.A. Tashkun, J. Vander Auwera, G. Wagner, J. Wilzewski, P. Wcisło, S. Yu, E.J. Zak, J. Quant. Spectrosc. Radiat. Transf. 203 (2017) 3–69.
[16] H. Zhang, J. Wu, P. Lu, J. Quant. Spectrosc. Radiat. Transf. 112 (2011) 220–229.
[17] N. Tasinato, G. Regini, P. Stoppa, A. Pietropolli Charmet, A. Gambi, J. Chem. Phys. 136 (2012) 214302.
[18] N. Tasinato, Int. J. Quantum Chem. 114 (2014) 1472–1485.
[19] P. Stoppa, N. Tasinato, A. Baldacci, A. Pietropolli Charmet, S. Giorgianni, F. Tamassia, E. Cané, M. Villa, J. Quant. Spectrosc. Radiat. Transf. 175 (2016) 8–16.
[20] J. Scaranto, D. Moro, N. Tasinato, P. Stoppa, S. Giorgianni, Spectrochim. Acta A 136 (2015) 1614–1620.
[21] K. Smith, D. Newnham, M. Page, J. Ballard, G. Duxbury, J. Quant. Spectrosc. Radiat. Transf. 56 (1996) 73–82.
[22] J.A. Beukes, F.N. Nicolaisen, J. Quant. Spectrosc. Radiat. Transf. 66 (2000) 185–198.
[23] E.J. Highwood, K.P. Shine, J. Quant. Spectrosc. Radiat. Transf. 66 (2000) 169–183.
[24] V. Orkin, A.G. Guschin, I.K. Larin, R.E. Huie, M.J. Kurylo, J. Photochem. Photobiol. A 157 (2003) 211–222.
[25] N. Tasinato, A. Turchetto, C. Puzzarini, P. Stoppa, A. Pietropolli Charmet, S. Giorgianni, Mol. Phys. 112 (2014) 2384–2396.
[26] N. Tasinato, S. Grimme, PCCP 17 (2015) 5659–5669.
[27] N. Tasinato, A. Turchetto, P. Stoppa, A. Pietropolli Charmet, S. Giorgianni, J. Chem. Phys. 142 (2015) 134310.
[28] N. Tasinato, A. Pietropolli Charmet, P. Stoppa, S. Giorgianni, G. Buffa, J. Chem. Phys. 132 (2010) 044315.
[29] N. Tasinato, A. Pietropolli Charmet, P. Stoppa, S. Giorgianni, G. Buffa, Spectrochim. Acta A 118 (2014) 373–379.
[30] N. Tasinato, A. Pietropolli Charmet, P. Stoppa, S. Giorgianni, Mol. Phys. 108 (2010) 677–685.
[31] N. Tasinato, A. Pietropolli Charmet, P. Stoppa, G. Buffa, C. Puzzarini, J. Quant. Spectrosc. Radiat. Transf. 130 (2013) 233–248.
[32] G. Ceselin, N. Tasinato, C. Puzzarini, A. Pietropolli Charmet, P. Stoppa, S. Giorgianni, J. Quant. Spectrosc. Radiat. Transf. 203 (2017) 367–376.
[33] G. Ceselin, N. Tasinato, C. Puzzarini, A. Pietropolli Charmet, P. Stoppa, S. Giorgianni, J. Quant. Spectrosc. Radiat. Transf. 198 (2017) 155–163.
[34] N. Tasinato, P. Stoppa, A. Pietropolli Charmet, S. Giorgianni, G. Buffa, A. Gambi, ChemPhysChem 12 (2011) 356–363.
[35] A.I. Nadezhdinskii, Spectrochim Acta A 52 (1996) 1041–1060.